Ultrathin self-assembled fibrin sheets

E. Tim O'Brien III[a,1], Michael R. Falvo[a], Daniel Millard[b], Brian Eastwood[c], Russell M. Taylor II[c], and Richard Superfine[a]

Departments of [a]Physics and Astronomy, [b]Biomedical Engineering, and [c]Computer Sciences, University of North Carolina, Chapel Hill, NC 27599-3255

Edited by José N. Onuchic, University of California at San Diego, La Jolla, CA, and approved October 16, 2008 (received for review May 20, 2008)

Fibrin polymerizes into the fibrous network that is the major structural component of blood clots and thrombi. We demonstrate that fibrin from three different species can also spontaneously polymerize into extensive, molecularly thin, 2D sheets. Sheet assembly occurs in physiologic buffers on both hydrophobic and hydrophilic surfaces, but is routinely observed only when polymerized using very low concentrations of fibrinogen and thrombin. Sheets may have been missed in previous studies because they may be very short-lived at higher concentrations of fibrinogen and thrombin, and their thinness makes them very difficult to detect. We were able to distinguish fluorescently labeled fibrin sheets by polymerizing fibrin onto micropatterned structured surfaces that suspended polymers 10 μm above and parallel to the cover-glass surface. We used a combined fluorescence/atomic force microscope system to determine that sheets were ≈5 nm thick, flat, elastic and mechanically continuous. Video microscopy of assembling sheets showed that they could polymerize across 25-μm channels at hundreds of μm^2/sec (≈10^{13} subunits/s·M), an apparent rate constant many times greater than those of other protein polymers. Structural transitions from sheets to fibers were observed by fluorescence, transmission, and scanning electron microscopy. Sheets appeared to fold and roll up into larger fibers, and also to develop oval holes to form fiber networks that were "preattached" to the substrate and other fibers. We propose a model of fiber formation from sheets and compare it with current models of end-wise polymerization from protofibrils. Sheets could be an unanticipated factor in clot formation and adhesion *in vivo*, and are a unique material in their own right.

clot | fiber | monomolecular sheet | network | thrombus

Because of the central role of fibrin in the clotting of blood during wound healing and in the formation of pathogenic vascular thrombi, the polymerization of fibrin has been actively studied since the mid-19th century (1). The parent protein, fibrinogen, is an elongated, sausage-shaped dimeric molecule with symmetry around a central globular domain (2–6). Cleavage and removal of the small peptides—fibrinopeptide A and later B—from fibrinogen by the enzyme thrombin expose specific binding sites ("knobs") on fibrin that allow binding to corresponding regions ("holes") on neighboring fibrin molecules (7–11). Fibrin can then self-associate to form elongated, sometimes twisted, often highly branched fibers and fiber networks that, together with platelets and blood cells, form clots in response to vascular injury (1, 12–15). Fibrin fibers are elastic and adhesive and show very high extensibility (16, 17). Recent studies suggest that these properties derive, at least in part, from the properties of the fibrin molecule itself (18–21). Exhaustive studies of fibrin polymerization *in vitro* have been carried out with purified components since the 1940s (e.g., 22, 23), but several details of fibrin assembly into fibers and fiber networks remain to be elucidated. Among the issues that are still actively being pursued are which domains within monomers are most responsible for the properties of the assembled fibers (5, 6, 12–14); how the polymerization process specifies branch points, branch densities, fiber thickness, and tension within clots; and how networks of fibers are formed without leaving free ends (14, 24–26).

In our system, we use micro-patterned structured surfaces (SSs) to generate plateaus and channels upon which fibrin fibers readily polymerize. We investigate the physical properties of fibers suspended across the 25-μm channels by using a combined fluorescence-atomic force microscope (AFM) system to monitor larger scale position and local fiber strain during pulls with the AFM tip (16, 17). The regular channels result in fibrin polymers being suspended *in situ* 10 μm above and parallel to the cover-glass surface. Fluorescently labeled polymers, even those that are only nanometers thick, can thus easily be distinguished from background surface fluorescence. In the present study we also polymerize fibrin directly on uncoated copper transmission electron microscope (TEM) grids, which similarly allows us to view polymer forms free of any support structures. We noticed that, when polymerizing very low concentrations of fibrinogen with low concentrations of thrombin, fiber formation sometimes appeared to be incomplete. Regions of the SS or grids showed uniform fluorescent structures over wide areas, as large as many thousands of μm^2, that were suspended above the cover-glass or between grid supports. In many regions these areas of uniform fluorescence transitioned into fibers, or had oval holes, which helped us to understand that the fluorescent areas were sheets of fibrin. After fibrin and thrombin were removed by dilution, even unfixed polymers were very stable and could thus be manipulated and measured under physiological buffer conditions.

In its broadest sense, fibrin sheets may represent a new class of biological membrane and protein polymer. Cellular lipid membranes are the only other form of naturally occurring extended 2D molecular-scale sheets thus far known. Fibrin sheets are fundamentally different from the fibrin films formed from compressed clots, as first described in the work of Ferry and Morrison (27). Whereas those films were made from compressed clots, the sheets we describe are able to self-assemble *in situ* at physiological pH and ionic strength, are molecularly thin and uniform, and require no outside forces or manipulation to form. Here we present the first description of fibrin sheets and their physical properties. We were also able to record movies of sheet polymerization on the SSs, using fluorescently labeled fibrinogen, and to obtain estimates of the rates of assembly. Finally, we use TEM of fixed samples to show that fibers and small fiber networks transition structurally from sheets, and describe a preliminary model of how this might take place.

Results

Physical Characteristics of Fibrin Sheets. Fibrin sheets were polymerized by adding ≈10 μl of human, mouse, or chicken fibrinogen directly to SSs (Fig. 1 *A* and *B*) or uncoated TEM grids (Fig. 1 *C* and *D*), and then adding an equal volume of human, mouse, or bovine thrombin to the fibrinogen. Final concentrations were 0.02 mg/ml (58 nM) fibrinogen and 0.1 U/ml thrombin. For human thrombin, our most routinely used type, 0.1 U/ml was ≈0.9 nM. This was approximately a 1:67 molar ratio of thrombin to fibrin, a ratio that suggests that thrombin was within the catalytic range. Polymerization took place in standard assembly buffers at neutral pH.

Author contributions: E.T.O., M.R.F., and R.S. designed research; E.T.O., M.R.F., and D.M. performed research; B.E. and R.M.T.I. contributed new reagents/analytic tools; E.T.O., M.R.F., D.M., B.E., R.M.T.I., and R.S. analyzed data; and E.T.O., M.R.F., and R.S. wrote the paper.

The authors declare no conflict of interest.

This article is a PNAS Direct Submission.

[1]To whom correspondence should be addressed. E-mail: etobrien@email.unc.edu.

This article contains supporting information online at www.pnas.org/cgi/content/full/0804865105/DCSupplemental.

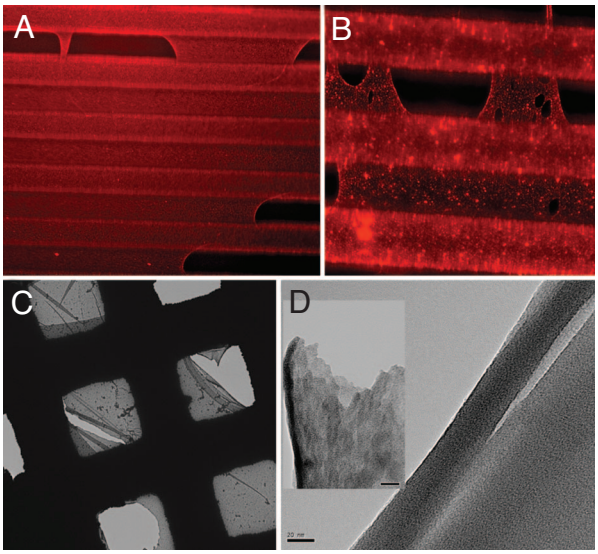

Fig. 1. Fibrin sheets are easily visible when suspended across gaps in SSs (*A* and *B*) or uncoated copper grids (*C* and *D*). Sheets in *A* and *B* are decorated with a 1/10,000 dilution of 24-nm fluorescent beads after the polymerization reaction was finished. Channels and plateaus (*A* and *B*) are 25 μm wide. *C* and *D* are TEM images of sheets assembled from chicken (*C*, magnification ×400) and human (*D*, magnification ×300,000) fixed specimens assembled *in situ* onto copper grids. Grid openings are 40 μm in *C* (scale bars, 20 nm in *D*).

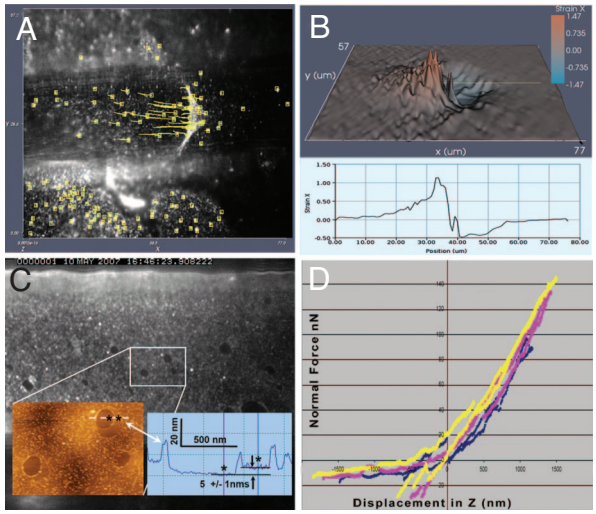

Fig. 2. Sheets are mechanically continuous. (*A*) Slice from a movie of a fluorescently labeled fibrin sheet. An AFM tip has touched the sheet and pulled it slowly toward the right to the maximum distance (shown). The lighter triangle shows the area of overlap of the sheet, and the yellow arrows are the distances displaced by tracked points (small squares) during the pull. (*B*) Strain field of the sheet at the time point in *A*. Strain is calculated for each pixel in the sheet, and the X component (parallel to SS) is displayed. The graph shows the strain versus distance data displayed in the figure. Maximum stain was approximately 146%. (*C*) Height data (*Inset*, *Left*) taken with the AFM within the area outlined in white on the background image. The background image was taken by a fluorescence microscope just before the image was taken with the AFM, using a combined AFM-light microscope. The height data (*Left*) shows the same three holes visible in fluorescence, and an area that was free of beads. The inset (*Right*) shows the graph of the height data from the SS plateau, across one bead, and then across approximately 200 nm of sheet before another bead is encountered. After the bead, the height again returns to approximately 5 nm. Black stars show the comparable positions in the insets. (*D*) Force data as the AFM tip was pressed into a suspended sheet approximately midway between the plateaus. The deflection of the calibrated tip was measured as force for each μm the sheet was displaced.

Sheets were seen with all combinations of fibrinogens and thrombin, both with and without any added Factor XIIIa, a transglutaminase that stabilizes monomer-monomer association (28). On the scale of light microscopy (Fig. 1 *A* and *B*), and low-magnification TEM imaging (Fig. 1*C*), we observed a characteristic "necking-down" of the sheets as they extended away from support surfaces. A minimum width was commonly observed toward the midpoint between attachments. Such attachments were not always between neighboring plateaus but in larger sheets could be several plateaus distant. The curved outline of sheet edges, very similar in shape to a catenary or parabola, was consistent with the sheet being under tension. We also found that the fibrin sheets tautly spanned the channels and grid spaces with large areas of uniform flatness, also consistent with the sheets between the plateaus being under tension, and implying mechanical continuity. An exception to sheet continuity was the presence of oval holes (Fig. 1*B*). These varied in size and number between preparations. They ranged from almost circular to distorted ovals, and, in unfixed samples, were always observed to have smooth boundaries.

On the nm scale, and excluding oval holes, sheets appeared to be continuous (Fig. 1*D*). No regular parallel gaps were seen, as might be expected for parallel protofibrils that were not bound together. Even at a magnification ×300,000, no gaps were observed in the fabric of the sheets (Fig. 1*D*). Moreover, the edges of fibrin films that were not torn always appeared smooth. In contrast, a torn, slightly rolled-up sheet can be seen to be smooth along the long edge, but rough along the broken edge (Fig. 1*D*, *Inset*; magnification ×300,000). This is consistent with the monomers being aligned within the sheet, and with the long axis of each subunit being parallel to the smooth edge. We also looked for any regular banding within sheets that might indicate a half staggered alignment. Previous studies have shown banding within fibers with a periodicity of ≈23 nm (29, 30), or approximately half the monomer length. This was interpreted as indicating a uniform and very regular half staggered arrangement, although later work argued that other arrangements of subunits could also produce the ≈23 nm period (31). We have not yet observed such a periodicity in sheets.

The mechanical integrity of unfixed sheets was confirmed by using a combined fluorescence-AFM system that allowed us to locate, image, measure, and manipulate the sheets (Fig. 2). A lateral pull of a sheet by the AFM tip demonstrated that strain was distributed continuously approximately 25 μm from the point of attachment to the tip. A movie was made of a sheet being pulled to the right, parallel to the SS plateaus with the AFM [Fig. 2A; see also supporting information (SI) Text and Movie S1]. The entire sequence was analyzed, from tip contact to maximum extension, and the displacement of each point that was able to be tracked during the pull was displayed as the lengths of yellow arrows. The smoothly varying distribution of strain is reversible and indicates the structure is a continuous elastic membrane. Displacements were seen up to 25 μm from the tip. At a rough size of 46 nm long, 10 nm wide per monomer, this is ≈500 monomer lengths, or ≈2,500 monomer widths from the point that force was applied. A plot of the strain in the direction parallel to the channel axis is also shown (Fig. 2*B*). A tilted 3D view of the strain data (Fig. 2*B*, *Upper*) and 2D plot of strain along the midline of the pull (Fig. 2*B*, *Lower*) shows that the strain falls off continuously from a maximum of 145% at the peak to half maximum at approximately 10 μm from the tip.

Imaging by AFM also was consistent with the sheet being molecularly flat and continuous. We imaged fluorescently labeled sheets in assembly buffer on the plateau of a SS (Fig. 2*C*, background), where we could be sure there was a sheet present and could identify particular areas with fewer fluorescent beads. AFM image data from the boxed area in the background image shows an area of film that had very few beads, within an oval hole. The height data, measured along the dashed line (Fig. 2*C*, *Left*, *Inset*), shows

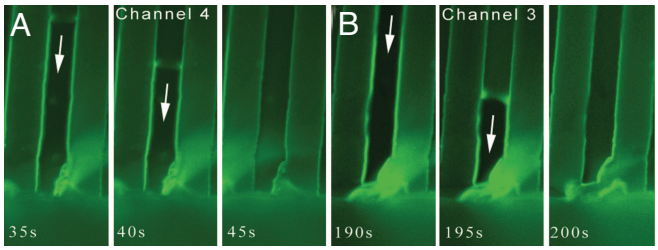

Fig. 3. Sheets rapidly polymerize across plateaus on SSs (downward). Two sequences, separated in time by 145 s, show assembly across two different channels, 4 and 3. Regions of interest from two sequences were taken at 5-s intervals for 7 min after adding thrombin (0.1 U/ml final concentration) to 0.02 mg/ml human fibrinogen. Alexa fluor 488-conjugated fibrinogen was mixed with non-labeled plasma fibrinogen before addition of the thrombin. Channels, numbered left to right in the field of view, are 20 μm wide. Approximately 120 μm vertical distance is in view in each channel. Arrows indicate where the sheet is about to polymerize. Five similar sequences were observed with nine intervals of appreciable polymerization.

a value of 5 $\pm$ 1 nm, both in the bead-free and bead-containing regions, with no gaps evident. This is interpreted as being one subunit in height (see *Discussion*). The uniformity of the AFM height data is consistent with our TEM data, in that the sheet appears by both methods to be uniform over hundreds of nanometers.

Vertical force versus displacement curves taken on sheets that had polymerized across the channels also showed behavior consistent with mechanical continuity (Fig. 2*D*). Here the force necessary to displace the sheet in the $-$Z direction was plotted, with different colors used to indicate individual approach and retraction curves. The slope was relatively linear in this region of forces, and reproducible, indicating that no structural damage (i.e., plastic deformation) had taken place in this displacement range. Initial estimates of the elastic modulus of these sheets based on our force curve data are consistent with earlier estimates of fibrin fibers and compressed films (19, 27) (i.e., within a few MPa). Together, AFM data strongly suggest that we are observing a continuous, planar, adhesive, elastic protein structure that may be only one subunit thick.

Kinetics of Sheet Assembly. Using fluorescently labeled human fibrinogen and adding thrombin to the microscope slide while viewing at room temperature, we were able to observe sheet formation on SSs in real time (Fig. 3). An EM CCD camera allowed us to reduce the intensity of excitation illumination and thus reduce photo-bleaching during extended viewing. In one sequence, all five channels that we observed were covered, one by one, by separate sheets (Movie S2 and *SI Text*). Two examples of sheets polymerizing "down" across an open channel, viewed at 5-s intervals, are displayed in Fig. 3. The sheets polymerized part of the way in the first interval, and the remaining distance during the second. Some of the assembly events appeared to finish with some overlap onto preceding sheets (e.g., Movie S2; central channel), indicating that, although sheets appear to assemble individually, nothing prevents them from assembling "on top" of preexisting sheets.

Nine assembly events were evaluated for the surface area of unsupported film covered per 5-s interval. Not including the sheet area that covered the plateaus (which would at least double the estimated value) or were out of the field of view, polymerization of fibrin films covered between 400 and 2,400 μm^2 of "empty" space between frames (mean, $\approx$250 μm^2/s). If we assume that each monomer covers approximately 46 $\times$ 10 nm in area, approximately 650,000 fibrin molecules per s were added at 0.02 mg/ml (60 nM) fibrinogen, for a pseudo-apparent first-order rate constant on the order of 10^{13} subunits/s·M. This value, approximately 10^4 to 10^7 higher than that estimated for the assembly of fibrin fibers (32), F-actin (33), or microtubules (34) implies, at least, that fibrin monomers were assembling at multiple sites simultaneously, and probably that fibrinogen had been concentrated on the SS or possibly on the assembling sheet itself. A relatively high concentration of monomer on the SSs and at the leading edge of the advancing sheets is consistent with our observation of a brighter fluorescence noted at that location (Fig. 3 *A* and *B*).

Transition of Sheets to Fibers. Fibers that stretched between plateaus generally had very uniform diameters, with edges that were smooth on the nm scale. However, fibers tended to flare out toward their region of attachment to the SS or TEM grid. These "root zones" were seen by negative stain TEM to be comprised of sheets in the process of rolling up, tearing, or folding (Fig. 4). Fig. 4 *A* and *B* show a low and higher magnification TEM view of a sheet that appeared to have rolled up in the mid-section between attachment areas (downward-facing arrows), and bunched up or gathered itself (upward-facing arrows). At higher magnification (Fig. 4*B*), the overlapping and gathered sheet is much clearer, and unfolded areas appear slightly textured, with darker threads present. A number of oval holes are also present (arrows), and the sheet appears to be breaking up. Sheets are also seen in the root zones of fibers on Fig. 4 *C–H*, as well as tears (Fig. 4 *C* and *G*) and abundant holes (Fig. 4 *D* and *H*). In some samples, very smooth root zones were seen, with no holes or tears (Fig. 4 *E* and *F*). The fiber in Fig. 4 *E* and *F* had broken from a striped grid on one end and was suspended from the remaining attachment. The root zone shows a sheet that had apparently folded in longitudinal creases parallel to the main fiber trunk. The step-wise, quantal nature of the intensity levels in the longitudinal bands (Fig. 4*F*, *Inset*), are consistent with accordion-like folds or pleats of a uniform parent sheet within this root zone. The straight, nearly parallel arrangement of the folds may imply alignment of subunits in the direction of the folds (see also Fig. 4*C*). An example of both tearing of a root zone sheet into smaller branches and the rolling-up of parts of the sheet onto these smaller fibers is seen in Fig. 4*G*. The small remnant connection to the grid is shown magnified in the inset (arrow points to the area that is magnified). Here the slightly irregular wrapping of the torn sheet can be seen. Finally, scanning EM also shows a broad sheet in the root zone across a SS channel, with many holes of various sizes, and pleats or ripples in the upper right corner (Fig. 4*H*). The fiber stayed straight and of uniform width for $\approx$25 μm until the other plateau was reached. Thus, in our system, the transition zones between attachment area and fibers appear to be comprised of folded, rolled, or torn sheets.

Discussion

We have shown that self-assembled fibrin sheets: (*i*) exist; (*ii*) can be very stable; (*iii*) can extend across gaps many microns wide; (*iv*) may be as thin as one subunit over extended areas; (*v*) can assemble with an extremely high apparent first-order rate constant; (*vi*) are mechanically continuous and elastic, with elastic properties consistent with measurements of fibers and compressed films; and (*vii*) appear to transition structurally into fibers and networks of fibers through a process of tearing, folding, and rolling, and the development of oval holes. These results have implications for current models of fibrin fiber assembly and possibly also for clot formation.

In our system, we observe that fibers and fiber networks always derive from root zones that appear to be sheets or sheet remnants. If it were true that fibers in our system derive from sheets, we should observe other indications of intermediate forms between sheets and fibers. Fig. 5 shows examples of transitional forms chosen from different samples or different areas within the same sample. These images show that fiber networks usually have outlines similar to that of a sheet of the same size, but with less of an obvious curve to the edges, as though the tension within the network was greater than that of the original sheet. Moreover, sheets can be seen that have few or no holes (Fig. 5 *A* and *D*; see also Figs. 1–3), a few holes (Fig. 5*B*, Fig. 1*B*, Fig. 2*C*, and Figs. 4 *B* and *D*), or many holes of various sizes (Fig. 4 *B–D*, *G*, and *H*), and these holes appear to leave behind

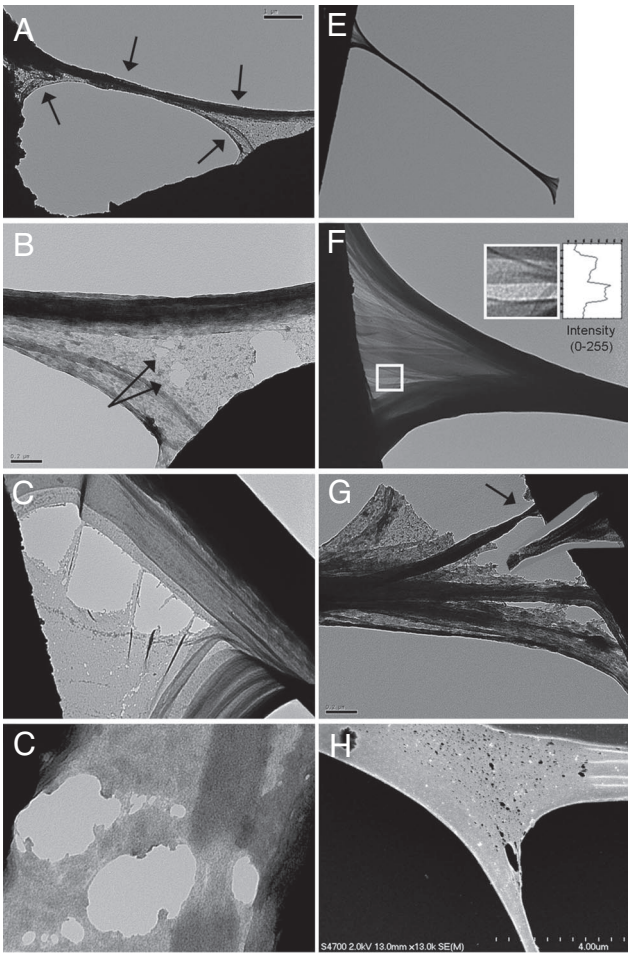

Fig. 4. Transmission (*A–G*) and scanning (*H*) EM images of fibrin fibers (*A* and *E*) and the root areas of fibers (*B–D*, *F*, and *G*). *A* and *B* and *E* and *F* are different magnification images of same fiber. Panels *B–D*, *G* and *H* show the very common appearance of tears (*C* and *G*) and oval holes (*B*, *D*, and *H*), even in these fixed samples. Fiber A/B show evidence of rolling up in the central portion (*A*; magnification ×8,800), and tearing in the root area (*B*, magnification ×40,000). (*C*) View (magnification ×19,500) of the root of chicken fiber, showing large tears and acute-angle folds of the parent sheet as it joins the main fiber shaft. (*D*) Root zone of a chicken fiber (magnification ×66,000) with multiple oval holes and areas that appear to have been pulling apart before fixation took place. The fiber in *E* (magnification ×530) and *F* (magnification ×8,800) was assembled on a ''grid'' with no cross-members. (*F*) Root zone in that fiber that extended for many microns to the right. Scan of intensity values and a higher magnification view of the scanned area (*Insets*) show the uniformity of density within a band, and the quantal nature of the transition between bands, consistent with folds or layers of films within the root zone as it transitions into the main fiber. (*G*) Root zone with areas that are torn from the grid appearing to roll up or fold onto the attached remainders (magnification ×40,000). The inset (magnification ×175,000) shows a close-up of the attached region at arrow. (*H*) SEM image (magnification ×4,700) shows the many holes in the root zone of mouse fiber assembled on an SS.

a few larger or many smaller linear attachments to other fibers or to the substrate (Fig. 5 *C* and *E*). These observations suggest that networks of fibers might evolve by the expansion of holes within a sheet that is already attached to a substrate.

A working model of the transition from sheet to fiber and to networks is summarized in Fig. 6, in comparison with a model of endwise assembly. Models of end-wise assembly of fibrin fibers suggest that monomers of fibrin assemble in a half-staggered, double-stranded protofibril that grows like a shoot or tree (Fig. 6 *A–D*) (23, 35, 36). As it elongates, it also widens by either aggregation of other protofibrils or by addition of monomers to lateral surfaces. Branching is thought to take place at random when a flaw develops in the staggered arrangement during protofibril or subunit addition (Fig. 6 *C* and *D*) (12–14, 26, 37, 38). End-wise assembly models do not readily explain how the extensively branched forms of fibrin networks develop and always connect even the finest fibers to another fiber or to the substrate without leaving occasional free ends (14, 24, 25). Although this is an important unanswered question for 3D clots, free fiber ends should be commonly observed on our SSs. Because the persistence length of fibrin fibers of the dimensions in our samples is millimeters (see *SI Text*), and our

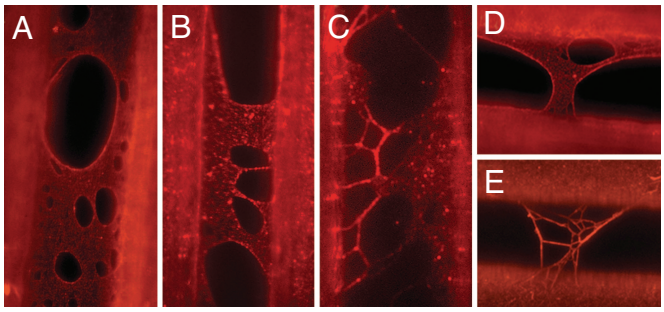

Fig. 5. Fluorescence light microscopic views of fiber networks in different stages of formation. *A–C* and *D–E* are roughly analogous forms.

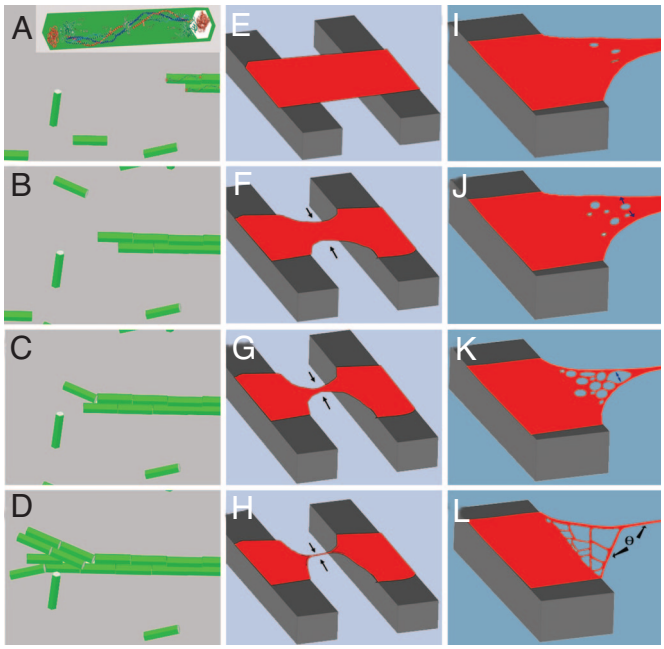

Fig. 6. Models of fibrin fiber development. (*A–D*) Protofibril attached (*Right*) and growing end-wise (*Left*). (*A*, *Inset*) Crystal structure of fibrin within a model of fibrin as a cylinder, which then assembles in a half-staggered pattern by addition of subunits. Branching occurs randomly at a point where the normal half-stagger is misaligned. (*E–H*) Formation of a larger fiber from the inward attractive forces of a fibrin sheet or film. After a film polymerizes, the attractive forces between the plateau and the sheet act to maintain the material in place, whereas the suspended film begins to gather or coalesce where it is not supported. The coalescence involves folding and rolling up of the free edges, and usually some tearing of the areas between the fiber and the plateau (the ''root'' areas). (*I–L*) Close-up of root zone with characteristic oval holes present. These gradually enlarge, with some tearing of the film, as a result of the same forces of self-attraction of the film, whereas the areas between the holes become secondary fibers, still attached to the main trunk. The obtuse angle (theta) between the main trunk and primary branches averages between 140° and 145°.

channels are only 25 μm across, one would predict that an appreciable proportion of fibers in a sample would be caught part way across the channel (see *SI Text*). This is especially true if the fiber had nucleated in solution and fallen at random onto the SS. But even if a fiber had nucleated on the SS and grew out over a channel, or randomly from the vertical surfaces, we would expect to see some free ends, especially at early time points. On the contrary, we almost never observe a free protruding fiber in unfixed specimens. Moreover, almost all fibers are found parallel to the plateau, with most exceptions taking place at the boundary of the SS and surrounding cover-glass.

A model wherein 2D fibrin sheets rapidly assemble across the channels and TEM grids and then roll up, fold, and tear apart into fibers and fiber networks readily explains our observations, although new questions present themselves. Fig. 6 *E–L* summarizes this model. Fibers appear to condense from narrow or wide sheets or films by a "drawing in" that, at some stage, involves folding or rolling of the sheet edges to form a central, main trunk or fiber (Fig. 6 *E–H*). As the main fiber condenses, oval holes and tears form in single monolayer parts of the root zones (Fig. 6 *I–L*). Areas of sheet that have folded or rolled into multiple layers appear to resist the incursion of the tears or holes as they enlarge, presumably because of additional bonding between the layers. This leaves a network of strands of multi-layered fibrin attaching the main fiber to the wall (Fig. 5 and Fig. 6 *I–L*). The proportion of larger to finer fibers would, in this model, depend on the geometry of attachment and rates of development of holes. This "sheet condensation" model has the virtue of explaining how networks form in arrangements in the plane of the plateaus and never leave free ends, but leaves for further experiments the question of how the sheets themselves are able to first nucleate themselves across the channels before extremely rapid assembly begins.

A model of fiber formation from the condensation of precursor sheets makes several further predictions that can be tested. A precursor sheet would have equal mass of material per square nm as well as equal mass of material per linear distance across the channel. If a sheet that extended across a channel (e.g., Fig. 6*E*) were to evolve into a fiber as drawn, we would predict that the mass of the resulting fiber per distance across the span would stay roughly constant. This implies that the mass/length ratio is conserved as one measures along a large fiber before a branch point or node, and then that mass/length is still constant as the total mass/length in the branches that derive from that node, continuing along that direction. Such a relationship is not predicted in the end-wise assembly model, as fibrin monomers may accrete at random anywhere along the length of the protofibril. Indeed, in the simplest end-wise model, the mass/length might be expected to double at a bifurcation, triple at a triple branch, and so on. More detailed observations will be needed to test the sheet condensation model, and more detailed models of sheet and fiber assembly may be able to include the effects of different rates of fibrin polymerization and different surface geometries.

Tension within fibrin fibers has been attributed to an inherently helical association of monomers as they bind to lateral faces of a protofibril (36). This association was suggested to produce tension as the protofibril shortens to allow favorable binding of new monomers, and also causes an intrinsic twist to the fiber. Our results show that planar fibrin polymers are under tension without any helical binding or twist, implying that other mechanisms must be capable of generating tension. Moreover, even very early studies show some fibers without twists (29), and we also observe some with twists and some without, but all appear to be under tension. Thus, our results suggest that tension derives from mechanisms other than helical monomer binding, such as inter-subunit rearrangement within the plane of the sheet or of the monomer after cleavage of fibrinopeptide A (39). Our data are also consistent with previous work that envisioned the association between fibrin monomers as being essentially planar (35). Whether the planarity is a consequence of our planar substrates (discussed later), the existence of sheets requires that inter-subunit and inter-protofibril bonding models must accommodate a planar polymer form, and suggests that the irregular twist seen in some fibers could be the result of uneven rolling-up of sheets as fibers form and not an inherent necessity of binding.

Our AFM measurement of a uniform height of a sheet over large distances, and the uniform density and quantal steps in density of sheets observed by TEM (Fig.1*D*, and Fig. 4 *C* and *F*), suggest that a monomolecular sheet is the primary form that assembles, but that multiple layers can form via folding of, rolling up of, or assembly onto, a parent sheet. The height we obtained (5 $\pm$ 1 nm) for an individual sheet (Fig. 2*C*) is larger than reported AFM measurements of individual fibrinogen monomers, with maximum values of 1 to 2 nm (40, 41). However, those authors and others (42) have shown that imaging of individual fibrin molecules is strongly affected by surface attraction and imaging conditions, and heights so obtained tend to be underestimates relative to estimates by crystal structure. Within a sheet, each subunit is supported through multiple interactions with neighboring monomers, and thus would be less distorted by surface effects. Our value is also close to the $\approx$ 6.5 nm value predicted from crystallography for chicken fibrinogen (6). Thus, although the sheet could be several layers thick, we believe it probable that the 5-nm region we measured reflects a single layer polymer of fibrin.

We have shown that fibrin can polymerize as a 2D membrane across at least 40 μm of unsupported space while anchored by flat surfaces. We have also observed sheets draping down from SSs to the cover-glass, and demonstrated that sheets are flexible and elastic. So although the range of curvatures under which sheets can form has not yet been determined, strictly planar supports are probably not necessary for sheet assembly. At the same time, we have not shown that sheets can polymerize far from surfaces, or that sheets have any role in fiber formation in 3D. Recent studies using light scattering and real-time fluorescence microscopy of clot formation *in vitro* argue that clots form by elongation of oligomers into protofibrils, followed by aggregation of protofibrils into fibers and branched networks (26). In this framework, sheets could represent an oligomeric form that is difficult to identify by those methods but which does play a very brief role in 3D fiber formation. Alternatively, sheets may not form at all without an organizing surface, arguing that fiber assembly away from surfaces takes place by very different kinetic pathways. Even if sheet formation *in vivo* is confined to the space very near surfaces, their formation could be a first step in clot formation at newly exposed subendothelial matrix after injury or dislodgment of a plaque, or on the surfaces of implanted vascular stents. AFM studies have shown that fibrinogen adheres to both hydrophobic and hydrophilic surfaces, but is oriented differently by each and is more strongly attracted to the former (40–42). In our study we see that fibrin sheets form and adhere to both hydrophobic polyurethane SSs, and relatively hydrophilic copper and glass. We therefore expect that sheets will be found to polymerize on most kinds of surfaces, but that the adhesive properties of a resulting sheet, and perhaps its orientation, could be affected by the hydrophobicity of the binding surface. If sheets were present at the adhesive interface of a clot, or fibers derived from sheets, such differences in adhesion could affect the chances of embolism. These possibilities will be very interesting to explore in future studies. Two SEM studies report finding sheet-like structures in human thrombi (43, 44), suggesting that a focused search for sheets in thrombi is warranted. However, any direct role of fibrin sheets in thrombogenesis remains to be established. If sheets did persist *in vivo* under some circumstances, our results suggest that they would be favored to form under conditions in which very slightly elevated amounts of active thrombin persist in a localized region. Such conditions could be present in areas with partially blocked blood flow and a stressed vascular wall, such as the deep veins of the leg. Clearly much more work will be needed to

determine whether this interesting new material has any physiologic role, either indirectly as a kinetic intermediate in fiber assembly, or directly as a structural or adhesive element in clot formation.

Materials and Methods

Human and mouse fibrinogens, human Factor XIII, and human and mouse thrombin were purchased from Enzyme Research Laboratories. The activity of human α-thrombin stock was 3,173 U/mg, 3.5 mg/ml (11,100 U/ml at 0.095 mM). Chicken fibrinogen was purified from fresh-frozen chicken plasma (a gift from Susan Lord, Chapel Hill, NC). Purified human, mouse, or chicken fibrinogen were dialyzed into10 mM Hepes, 150 mM NaCl buffer, pH 7.4, at 0.6 mg/ml and frozen in small aliquots at $-80°$. Aliquots were then diluted to 0.04 mg/ml, placed on SSs, and an equal volume of freshly diluted human, mouse, or bovine thrombin at 0.2 U/ml in 10 mM $CaCl_2$ Hepes buffer was added. Factor XIII (1 μg/ml final) was present in most reactions. SSs in humid chambers were then placed at 37° for 2 h. Samples were then washed with buffer, and a 1/10,000 dilution of 20 nm red fluorescent beads (Invitrogen) were added for 5 min, washed again, and viewed. SSs were made as described previously (6, 7), by using Norland Optical 81 polymerized into polydimethylsiloxane stamps on cover-glass surfaces. TEM samples were assembled in parallel with SS samples directly onto uncoated grids or stripes, but 0.2% glutaraldehyde was used as fixative, with or without tannic acid present (1%), with 1% uranyl acetate used as a stain. Vapor deposited OsO_4 was used in preparation of Fig. 1*C*. The AFM (Explorer; Veeco), positioned on the stage of an inverted epifluorescence microscope, enabled simultaneous AFM manipulation and optical data acquisition. Olympus Biolever cantilevers (spring constant, 0.03 N/m) were used for manipulation and imaging in liquid in AC mode. Manipulations were performed using nanoManipulator software (3rd Tech). Live fibrin assembly took place by addition of a 2% M/M Alexa-fluor 488 (Invitrogen)-labeled human fibrinogen to unlabeled human fibrinogen under standard conditions without Factor XIII, with thrombin added to the sample on microscope stage. Frames were collected every 5 s using a Cascade II camera (Photometrics) on medium gain, with a $\times$1/10 neutral density filter and a 25 $\times$ 0.8 numerical aperture Zeiss objective).

ACKNOWLEDGMENTS. We thank the University of North Carolina-Chapel Hill Fibrin Discussion Group for helpful feedback and discussion, Dr. Susan Lord for critical reading of the manuscript; Susan, Dr. Oleg Gorkun, and Lifang Ping for fibrinogens, protocols, and discussion; Robert Campbell and Dr. Alisa Wolberg for AlexaFluor fibrinogen; Johnathan Houser for AFM manipulation of fibrin sheets for Fig. 2; Margaret O'Brien for help in making samples, reading the manuscript, and helpful discussions; and Tim O'Brien IV for help formatting images in PhotoShop. This work was supported by National Science Foundation Proposal 0705977 and by National Institute of Biomedical Imaging and Bioengineering resource award P41-EB002025–23A1 supporting Computer Integrated Systems for Microscopy and Manipulation (CISMM).

1. Blomback B (2001) Fibrinogen: evolution of the structure-function concept. *Ann N Y Acad Sci* 936:1–10.
2. Hall CE, Slayter HS (1959) The fibrinogen molecule, its size, shape and mode of polymerization. *J Biophys Biochem Cytol* 5:11–17.
3. Fowler WE, Erickson HP (1979) Trinodular structure of fibrinogen. Confirmation by both shadowing and negative stain electron microscopy. *J Mol Biol* 134:241–249.
4. Williams RC (1981) Morphology of bovine fibrinogen monomers and fibrin oligomers. *J Mol Biol* 150:399–408.
5. Brown JH, Volkmann N, Jun G, Henschen-Edman AH, Cohen C (2000) The crystal structure of modified bovine fibrinogen. *Proc Natl Acad Sci USA* 97:85–90.
6. Yang Z, Kollman JM, Pandi L, Doolittle RF (2001) Crystal structure of native chicken fibrinogen at 2.7 A resolution. *Biochemistry* 40:12515–12523.
7. Lorand L (1951) "Fibrino-peptide'; new aspects of the fibrinogen-fibrin transformation. *Nature* 167:992–993.
8. Laudano AP, Doolittle RF (1978) Synthetic peptide derivatives that bind to fibrinogen and prevent the polymerization of fibrin monomers. *Proc Natl Acad Sci USA* 75:3085–3089.
9. Pratt KP, Cote HC, Chung DW, Stenkamp RE, Davie EW (1997) The primary fibrin polymerization pocket: three-dimensional structure of a 30-kDa C-terminal gamma chain fragment complexed with the peptide Gly-Pro-Arg-Pro. *Proc Natl Acad Sci USA* 94:7176–7181.
10. Everse SJ, Spraggon G, Veerapandian L, Riley M, Doolittle RF (1998) Crystal structure of fragment double-D from human fibrin with two different bound ligands. *Biochemistry* 37:8637–8642.
11. Litvinov RI, Gorkun OV, Owen, SF Suman H, Weisel JW (2005) Polymerization of fibrin: specificity, strength, and stability of knob-hole interactions studied at the single-molecule level. *Blood* 106:2944–2951.
12. Mosesson WW (2005) Fibrinogen and fibrin structure and functions. *J Thromb Haemost* 3:1894–1904
13. Lord ST (2007) Fibrinogen and fibrin: scaffold proteins in hemostasis. *Curr Opin Hematol*. 14:236–241.
14. Weisel JW (2007) Structure of fibrin: impact on clot stability. *J Thromb Haemost 5* 1:116–124.
15. Wolberg AS, Campbell RA (2008) Thrombin generation, fibrin clot formation and hemostasis. *Transfus Apher Sci* 38:15–23.
16. Guthold M, *et al.* (2004) Visualization and mechanical manipulations of individual fibrin fibers suggest that fiber cross section has fractal dimension 1.3. *Biophys J* 87:4226–4236.
17. Liu W, *et al.* (2006) Fibrin fibers have extraordinary extensibility and elasticity. *Science* 313:634.
18. Marguerie G, Stuhrmann HB (1976) A neutron small-angle scattering study of bovine fibrinogen. *J Mol Biol* 102:143–156.
19. Collet JP, Shuman H, Ledger RE, Lee S, Weisel JW (2005) The elasticity of an individual fibrin fiber in a clot. *Proc Natl Acad Sci USA* 102:9133–9137.
20. Brown AE, Litvinov RI, Discher DE, Weisel JW (2007) Forced unfolding of coiled-coils in fibrinogen by single-molecule AFM. *Biophys J* 92:L39–L41.
21. Lim BB, Lee EH, Sotomayor M, Schulten K (2008) Molecular basis of fibrin clot elasticity. *Structure* 16:449–459.
22. Ferry JD, Morrison, PR (1947) Preparation and properties of serum and plasma Proteins. VIII: the conversion of human fibrinogen to fibrin under various conditions *J Am Chem Soc* 69:388–400.
23. Ferry JD (1954) Polymerization of fibrinogen. *Physiol Rev* 34:753–760.
24. Weisel JW, Nagaswami C (1992) Computer modeling of fibrin polymerization Kinetics correlated with electron microscope and turbidity observations: clot structure And assembly are kinetically controlled. *Biophys J* 63:111–128.
25. Ryan EA, Mockros LF, Weisel JW, Lorand L (1999) Structural origins of fibrin clot rheology. *Biophys J* 77:2813–2826.
26. Chernysh IN, Weisel JW (2008) Dynamic imaging of fibrin network formation correlated with other measures of polymerization. *Blood* 111:4854–4861.
27. Ferry JD, Morrison PR (1947) Preparation and properties of serum and plasma proteins. IX: human fibrin in the form of an elastic film. *J Am Chem Soc* 69:400–409.
28. Standeven KF, *et al.* (2007) Functional analysis of fibrin {gamma}-chain cross-linking by activated factor XIII: determination of a cross-linking pattern that maximizes clot stiffness. *Blood* 110:902–907.
29. Porter KR, Hawn CV (1949) Sequences in the formation of clots from purified bovine fibrinogen and thrombin; a study with the electron microscope. *J Exp Med* 90:225–232.
30. Hall CE (1949) Electron microscopy of fibrinogen and fibrin. *J Biol Chem* 179:857–865.
31. Hunziker EB, Straub PW, Haeberli A (1990) A new concept of fibrin formation based upon the linear growth of interlacing and branching polymers and molecular alignment into interlocked single-stranded segments. *J Biol Chem* 265:7455–7463.
32. Lewis SD, Shields PP, Shafer J (1985) Characterization of the kinetic pathway for liberation of fibrinopeptides during assembly of fibrin. *J Biol Chem* 260:10192–10199.
33. Kuhn J, Pollard T (2005) Real-time measurements of actin filament polymerization by total internal reflection fluorescence microscopy. *Biophys J* 88:1387–1402.
34. Walker RA, *et al.* (1988) Dynamic instability of individual microtubules analyzed by video light microscopy: rate constants and transition frequencies. *J Cell Biol* 107(4):1437–1448.
35. Fowler WE, Hantgan RR, Hermans J, Erickson HP (1981) Structure of the fibrin protofibril. *Proc Natl Acad Sci USA* 78:4872–4876.
36. Weisel JW, Nagaswami C, Makowski L (1987) Twisting of fibrin fibers limits their radial growth. *Proc Natl Acad Sci USA* 84:8991–8995.
37. Voter WA, Lucaveche C, Blaurock AE, Erickson HP (1986) Lateral packing of protofibrils in fibrin fibers and fibrinogen polymers. *Biopolymers* 25:2359–2373.
38. Mosesson MW, DiOrio JP, Siebenlist KR, Wall JS, Hainfeld JF (1993) Evidence for a second type of fibril branch point in fibrin polymer networks, the trimolecular junction. *Blood* 82:1517–1521.
39. Evans-Nguyen KM, *et al.* (2006) Changes in adsorbed fibrinogen upon conversion to fibrin. *Langmuir* 22:5115–5121.
40. Marchin KL, Berrie CL (2003) Conformational changes in the plasma protein fibrinogen upon adsorption to graphite and mica investigated by atomic force microscopy. *Langmuir* 19:9883–9888.
41. Agnihotri A, Siedlecki CA (2004) Time-dependent conformational changes in fibrinogen measured by atomic force microscopy. *Langmuir* 20:8846–8852.
42. Ta TC, Sykes MT, McDermott MT (1998) Real-time observation of plasma protein film formation on well-defined surfaces with scanning force microscopy. *Langmuir* 14:2435–2443.
43. Smith RR, Russell WF, Percy ML (1980) Ultrastructure of carotid plaques. *Surg Neurol* 14:145–153.
44. Pretorius E, Briedenhann S, Marx J, Franz RC (2006) Structural changes in the fibrin network of a pretoria family with dysfibrinogenemia: a scanning electron microscopical study. *Ultrastruct Pathol* 30:167–176.